The EMBO Journal (2011) 30, 3052–3064 | © 2011 European Molecular Biology Organization | All Rights Reserved 0261-4189/11
www.embojournal.org

THE EMBO JOURNAL

Sch9 regulates ribosome biogenesis via Stb3, Dot6 and Tod6 and the histone deacetylase complex RPD3L

Alexandre Huber[1], Sarah L French[2], Hille Tekotte[3], Seda Yerlikaya[1], Michael Stahl[1], Mariya P Perepelkina[1], Mike Tyers[3], Jacques Rougemont[4], Ann L Beyer[2] and Robbie Loewith[1,*]

[1]Department of Molecular Biology and National Center for Competence in Research Program 'Frontiers in Genetics', University of Geneva, Geneva, Switzerland, [2]Department of Microbiology, University of Virginia Health System, Charlottesville, VA, USA, [3]Wellcome Trust Center for Cell Biology, University of Edinburgh, Edinburgh, Scotland and [4]Bioinformatics and Biostatistics Core Facility, Swiss Federal School of Engineering of Lausanne and Swiss Institute of Bioinformatics, Lausanne, Switzerland

TORC1 is a conserved multisubunit kinase complex that regulates many aspects of eukaryotic growth including the biosynthesis of ribosomes. The TOR protein kinase resident in TORC1 is responsive to environmental cues and is potently inhibited by the natural product rapamycin. Recent characterization of the rapamycin-sensitive phosphoproteome in yeast has yielded insights into how TORC1 regulates growth. Here, we show that Sch9, an AGC family kinase and direct substrate of TORC1, promotes *ribosome biogenesis* (*Ribi*) and *ribosomal protein* (*RP*) gene expression via direct inhibitory phosphorylation of the transcriptional repressors Stb3, Dot6 and Tod6. Deletion of *STB3*, *DOT6* and *TOD6* partially bypasses the growth and cell size defects of an *sch9* strain and reveals interdependent regulation of both *Ribi* and *RP* gene expression, and other aspects of Ribi. Dephosphorylation of Stb3, Dot6 and Tod6 enables recruitment of the RPD3L histone deacetylase complex to repress *Ribi/RP* gene promoters. Taken together with previous studies, these results suggest that Sch9 is a master regulator of ribosome biogenesis through the control of *Ribi*, *RP*, *ribosomal RNA* and *tRNA* gene transcription.

The EMBO Journal (2011) **30,** 3052–3064. doi:10.1038/emboj.2011.221; Published online 5 July 2011
Subject Categories: signal transduction; chromatin & transcription
Keywords: rapamycin; ribosome biogenesis; RPD3 histone deacetylase; Sch9; Stb3

*Corresponding author. Department of Molecular Biology, University of Geneva, 30, quai Ernest-Ansermet, Geneva 1211, Switzerland. Tel.: +41 22 379 6116; Fax: +41 22 379 6868;
E-mail: robbie.loewith@unige.ch

Received: 3 January 2011; accepted: 8 June 2011; published online: 5 July 2011

Introduction

The budding yeast *Saccharomyces cerevisiae* synthesizes ~2000 ribosomes per minute per cell under optimal growth conditions. To ensure the proper transcription, processing and assembly of the 78 ribosomal proteins (RPs) and 4 ribosomal RNAs (rRNAs) that constitute a ribosome, hundreds of *trans*-acting assembly factors and other cofactors for translation regulation, tRNA biosynthesis or purine/pyrimidine synthesis must also be produced from a set of coregulated genes known as the *ribosome biogenesis* (*Ribi*) regulon (Jorgensen *et al*, 2004; Wade *et al*, 2006). Ribosome biogenesis thus requires the coordinated activities of all three RNA polymerases (RNAPI, II and III) and can commandeer up to 70–80% of total nuclear transcriptional capacity (Warner, 1999). To limit unnecessary energy expenditure under stress and/or starvation conditions, the synthesis of ribosomal components and their Ribi cofactors must be tightly controlled. This regulation is imposed in part by nutrient- and stress-sensitive signalling networks. Most notably, the TOR and PKA kinases regulate Ribi at the transcriptional level (De Virgilio and Loewith, 2006).

The TOR kinases in yeast (TOR1 and TOR2) are the catalytic subunits of two functionally distinct multiprotein complexes, TORC1 and TORC2 (De Virgilio and Loewith, 2006). In optimal growth conditions, TORC1 is active and promotes growth both by stimulating anabolic processes, such as protein synthesis, and by inhibiting catabolic processes, such as macroautophagy (De Virgilio and Loewith, 2006). Binding of the natural product macrolide rapamycin or exposure to cellular stress rapidly inactivates TORC1 (Heitman *et al*, 1991; Urban *et al*, 2007), inhibits anabolic processes and induces catabolic processes.

Ribosome biogenesis is the principal anabolic process that is stimulated by TORC1. The assembly of new ribosomes begins with the TORC1-dependent activation of RNAPI, II and III to promote the transcription of *rRNA*, *RP* and *Ribi*, and *tRNA* genes, respectively (Zaragoza *et al*, 1998; Jorgensen *et al*, 2004; Martin *et al*, 2004; Schawalder *et al*, 2004; Wade *et al*, 2004; Rudra *et al*, 2005). TORC1-dependent signals are mediated by a number of effectors kinases (Breitkreutz *et al*, 2010), the best characterized of which is Sch9, an AGC family Ser/Thr kinase and direct substrate of TORC1 (Urban *et al*, 2007). Sch9 regulates RNAPIII by phosphorylating and inactivating Maf1, a conserved repressor of RNAPIII activity (Upadhya *et al*, 2002; Oficjalska-Pham *et al*, 2006; Roberts *et al*, 2006; Huber *et al*, 2009; Lee *et al*, 2009; Wei and Zheng, 2009). TORC1 also stimulates RNAPI in both an Sch9-dependent and -independent manner, in part through regulation of the transcription initiation factor Rrn3 (Peyroche *et al*, 2000; Laferte *et al*, 2006; Huber *et al*, 2009). Finally, TORC1 regulates the activity of RNAPII at the large cohort of *Ribi* and *RP* genes, at least in part via Sch9 (Jorgensen *et al*, 2004; Urban *et al*, 2007).

Ribi and *RP* genes exhibit overlapping but non-identical kinetics of regulation due to their differing promoter structures, which bind both common and distinct transcription factors (Ju and Warner, 1994; Hughes *et al*, 2000; Jorgensen *et al*, 2004; Wade *et al*, 2006; Lempiainen and Shore, 2009). Among these factors, Fhl1/Ifh1/Crf1, Sfp1 and Hmo1 have all been shown to mediate TORC1 signals to *RP* and/or *Ribi* genes (Jorgensen *et al*, 2004; Martin *et al*, 2004; Schawalder *et al*, 2004; Wade *et al*, 2004; Rudra *et al*, 2005; Lempiainen *et al*, 2009; Singh and Tyers, 2009). However, genetic analysis suggests that Sch9 functions in parallel to Fhl1/Ifh1 and Sfp1 (Jorgensen *et al*, 2004; Lempiainen *et al*, 2009), by an as yet undeciphered mechanism.

Ribi gene promoters are enriched in two distinct motifs, the PAC element (Polymerase A and C) and the RRPE element (rRNA processing element) (Hughes *et al*, 2000; Jorgensen *et al*, 2004; Wade *et al*, 2006). Several independent studies recently identified two Myb-like HTH transcription factors, Dot6 and Tod6, as cognate factors for the PAC element (Badis *et al*, 2008; Freckleton *et al*, 2009; Zhu *et al*, 2009). Dot6 and Tod6 act as transcriptional repressors whose function is antagonized by signals from TORC1, Sch9 and PKA (Lippman and Broach, 2009). Despite its apparent lack of a DNA-binding domain, Stb3 recognizes the RRPE element, where it can apparently act as either a transcriptional activator (Liko *et al*, 2007) or a transcriptional repressor (Liko *et al*, 2010), depending on growth context. Like Dot6 and Tod6, Stb3 appears to lie downstream of the TORC1–Sch9 axis (Liko *et al*, 2010).

Histone acetylation within *Ribi* and *RP* gene promoters is also regulated by TORC1. Inhibition of TORC1 by rapamycin induces both the release of the Esa1 histone acetyltransferase and the recruitment of the Rpd3 histone deacetylase at *RP* gene promoters, and thereby represses transcription (Rohde and Cardenas, 2003; Humphrey *et al*, 2004). Rpd3 is also recruited to *Ribi* gene promoters upon TORC1 inhibition (Humphrey *et al*, 2004). Importantly, in the absence of Rpd3, but not other histone deacetylases, rapamycin effectively fails to repress both *RP* and *Ribi* regulons (Humphrey *et al*, 2004). Rpd3 resides in two functionally distinct complexes, RPD3L and RPD3S, which are characterized by specific essential subunits such as Sds3 and Sap30 (RPD3L) and Rco1 (RPD3S) (Carrozza *et al*, 2005b). RPD3S is thought to suppress spurious intragenic transcription by deacetylating histones in coding regions, while RPD3L functions to repress transcription initiation when recruited to promoter regions by various DNA-binding factors (Carrozza *et al*, 2005a, b).

The mechanism whereby TORC1 controls the *Ribi* and *RP* regulons remains only poorly characterized. Our recent analysis of the rapamycin-sensitive phosphoproteome revealed that Stb3, Dot6 and Tod6 become hypophosphorylated upon TORC1 inhibition in an Sch9-dependent manner, suggesting that these factors may be the missing effectors of TORC1 in the control of RNAPII-mediated transcription of *Ribi* and *RP* genes (Huber *et al*, 2009). Consistently, rapamycin treatment elicited dephosphorylation of Stb3 and Dot6 in a similar survey for novel TORC1 effectors (Soulard *et al*, 2010). Here, we demonstrate that Sch9 directly phosphorylates the Stb3, Dot6 and Tod6 transcription factors to abrogate the repression of *Ribi* and *RP* genes. Upon Sch9 inhibition, Stb3 and Dot6/Tod6 cooperate to recruit the RPD3L histone deacetylase complex to *Ribi* gene promoters, whereas Stb3 is responsible for recruitment of RPD3L to *RP* gene promoters. These observations consolidate the TORC1- and Sch9-dependent mechanisms of transcriptional regulation of the major promoter classes during ribosome biogenesis.

Results

Sch9 directly phosphorylates Stb3, Dot6 and Tod6 in vivo and in vitro

We first sought to determine whether the TORC1-dependent phosphorylation of Stb3, Dot6 and Tod6 is specifically mediated by Sch9. We also included PKA in these analyses as PKA has been shown previously to phosphorylate Stb3 and Dot6 *in vitro* (Budovskaya *et al*, 2005; Deminoff *et al*, 2006) and this kinase often has overlapping functions with Sch9 (De Virgilio and Loewith, 2006; Zaman *et al*, 2008; Ramachandran and Herman, 2011). We used analogue-sensitive alleles of *SCH9* ($sch9^{as}$) and *PKA* (pka^{as}: $tpk1^{as}tpk2^{as}tpk3^{as}$ as PKA activity is encoded by three partially redundant *TPK* genes in yeast) (Jorgensen *et al*, 2004; Yorimitsu *et al*, 2007), which encode a point mutation in the kinase domain that specifically renders the enzyme sensitive to inhibition by the bulky ATP analogue 1NM-PP1 (Shokat and Velleca, 2002). We observed that HA-tagged Stb3 analysed from untreated cells migrated as a smear in SDS–PAGE, suggesting phosphorylation on multiple sites (Supplementary Figure S1). This migration pattern was not dramatically altered by rapamycin treatment or by inhibition of $Sch9^{as}$ and/or PKA^{as} with 1NM-PP1 (Figure 1A; Supplementary Figure S1). We and others have previously observed that Sch9 and PKA share preferences for Ser/Thr residues preceded by an Arg at the −3 position and Arg/Lys at −2, that is, a consensus motif of R[R/K]x[S/T]* (Huber *et al*, 2009; Lee *et al*, 2009). We probed for potential changes in Stb3 phosphorylation using an antibody against this phosphorylated consensus motif (see Supplementary Figure S1A for antibody specificity controls). We observed rapid dephosphorylation of Stb3 after Sch9 inhibition but not after PKA inhibition, suggesting that Stb3 phosphorylation at the consensus R[R/K]x[S/T] sites is specifically regulated by Sch9 *in vivo* (Figure 1A). Inhibition of either Sch9 or PKA also resulted in an apparent rapid dephosphorylation of both Dot6 (Figure 1B) and Tod6 (Figure 1C). Combined inhibition of the two kinases caused a more pronounced dephosphorylation of both substrates, suggesting that Sch9 and PKA act in parallel on Dot6 and Tod6.

To determine if the three transcription factors might be direct substrates of Sch9, recombinant Stb3, Dot6 and Tod6 were tested for their ability to be phosphorylated by Sch9 in an *in vitro* kinase assay. A constitutively active form, $Sch9^{3E}$ (Urban *et al*, 2007), but not catalytically impaired Sch9, could directly phosphorylate all three proteins *in vitro* (Figure 1D–G). Together, these *in vivo* and *in vitro* results suggest that Sch9 directly phosphorylates Stb3, Dot6 and Tod6.

Sch9 regulates Ribi and RP genes via Stb3, Dot6, Tod6 and the histone deacetylase RPD3L

Next, we wished to examine the biological function for Stb3, Dot6 and Tod6 phosphorylation downstream of TORC1/Sch9. Dot6 and Tod6 function as repressors of *Ribi/RP* transcription (Lippman and Broach, 2009) presumably via their intrinsic affinity for PAC promoter elements, which are enriched upstream of *Ribi* genes (Freckleton *et al*, 2009; Zhu *et al*, 2009).

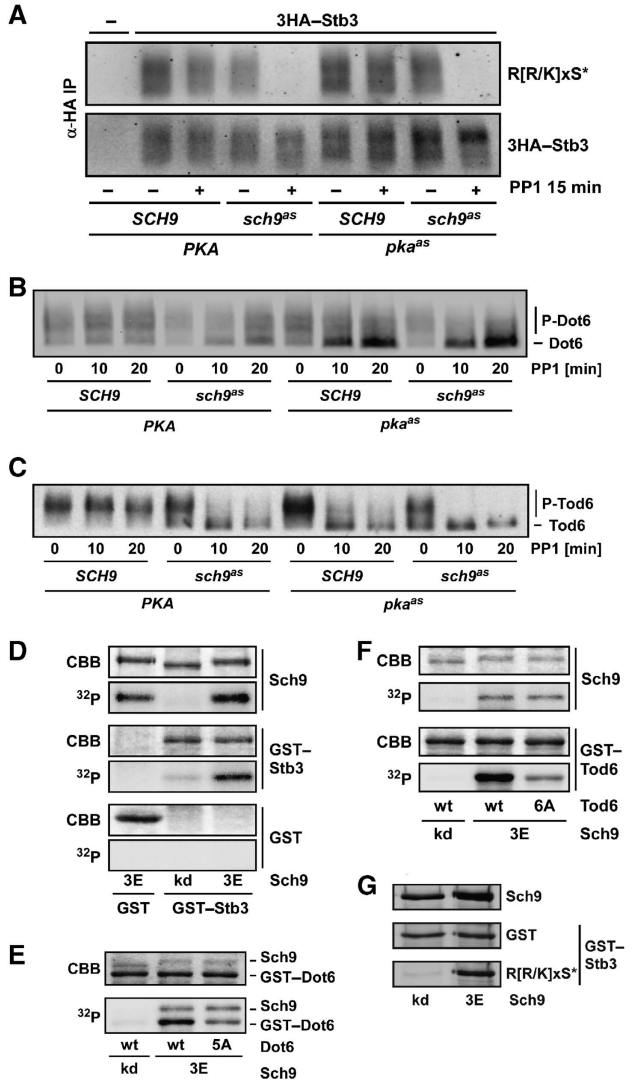

Figure 1 Stb3, Dot6 and Tod6 are directly phosphorylated by Sch9 *in vivo* and *in vitro*. (**A**–**C**) Strains of indicated genotype and expressing 3HA–Stb3 (**A**), Dot6–5HA (**B**) or Tod6–5HA (**C**) were grown exponentially in YPD at 30°C and subjected to the indicated treatments. (**A**) 3HA–Stb3 was immunoprecipitated after denaturing protein extraction and phosphorylation status (anti-R[R/K]xS*) and abundance (anti-HA) determined by western blot. A strain transformed with empty vector was used as a mock IP control (left lane) (**B**, **C**) Dot6–5HA and Tod6–5HA phosphorylation status was determined by migration in SDS–PAGE and anti-HA western blot. (**D**–**G**) *In vitro* kinase assays. GST–Stb3 (**D**, **G**), GST–Dot6^{wt} and GST–Dot6^{5A} (**E**) and GST–Tod6^{wt} and GST–Tod6^{6A} (**F**) were tested as substrates for Sch9^{3E} (Urban *et al*, 2007) in presence of γ-^{32}P-ATP (**D**–**F**) or unlabelled ATP only (**G**). Reactions with GST as the substrate (**D**) or Sch9^{kd}, a point mutant lacking catalytic activity, as the kinase (**D**–**G**) were performed to control for specificity. Reactions were resolved by SDS–PAGE, stained with coomassie (CBB) and ^{32}P incorporation detected by autoradiography (**D**–**F**). Alternatively, reactions were analysed by western blot against the Protein A and GST tags and the phosphorylated R[R/K]x[S/T]* motif (**G**).

Stb3 also appears to function as a downstream transcriptional effector of Sch9, but curiously seems to act as both a transcriptional activator and repressor (Liko *et al*, 2007, 2010). To clarify the role of Stb3 and to comprehensively characterize the functional relationships of Stb3, Dot6 and Tod6 as downstream effectors of Sch9, we used mRNA-Seq transcriptome profiles to delineate the sets of genes that respond to each factor. As expected (Jorgensen *et al*, 2004), inhibition of Sch9 resulted in downregulation of many genes (12% of 5025 genes detected were downregulated >1.5-fold), among which *Ribi* (79% of 457 genes; $P<10^{-31}$) and *RP* (99% of 137 genes; $P<10^{-37}$) genes were highly enriched (Figure 2A). As observed in the mRNA-Seq data and confirmed by RT–qPCR (Supplementary Figure S2A and B), this repression was partially alleviated when *STB3* or *DOT6* and *TOD6* were deleted. This effect was not due to a prior lack of induction of the *Ribi*/*RP* genes in these deletion strains (Supplementary File F1 and data not shown). Strikingly, disruption of *STB3* abrogated the repression of *RP* genes following Sch9 inhibition ($P<10^{-37}$; Figure 2A; Supplementary Figure S2A–C; Supplementary Table S1); conversely Sch9 appeared to regulate *Ribi* genes preferentially via Dot6 and Tod6 ($P<10^{-31}$). The combined deletion of all three factors had an additive effect, as observed by the near total failure of Sch9 inhibition to repress *Ribi*/*RP* gene expression in the *stb3*Δ *dot6*Δ *tod6*Δ background. In agreement with the known DNA motif preferences, *Ribi* genes that harboured only RRPE elements in their promoters were preferentially regulated via Stb3 ($P<10^{-4}$; Figure 2A; Supplementary Figure S2C; Supplementary Table S1), whereas genes bearing only PAC elements were preferentially regulated by Dot6/Tod6 ($P<0.001$).

In addition to these effects, we observed hyper-induction of Gcn4 target genes upon Sch9 inhibition in a *dot6*Δ *tod6*Δ strain and to an even greater extent in a *stb3*Δ strain (Supplementary Figure S2B). Although we have not pursued this effect further, we suspect that imbalanced repression of *Ribi* genes under these conditions may result in increased *GCN4* mRNA translation, and consequently in the observed increase in expression of Gcn4 targets.

Stb3 was originally identified as a binding partner of Sin3 (Kasten and Stillman, 1997), a component of the RPD3L and RPD3S histone deacetylase complexes. Dot6 and Tod6 also bind to the RPD3L complex (Shevchenko *et al*, 2008). In addition, Rpd3, which is the shared catalytic subunit of these deacetylase complexes, is implicated in *Ribi* and *RP* gene regulation downstream of TORC1 (Rohde and Cardenas, 2003; Humphrey *et al*, 2004). The interaction of Stb3, Dot6 and Tod6 with RPD3 could thus explain their reported activities as transcriptional repressors. We, therefore, determined whether either of the RPD3 complexes function downstream of Sch9 in the regulation of *Ribi*/*RP* genes. We examined the transcriptional profile caused by Sch9 inhibition in strains that lacked Rpd3, Rco1 (a specific and essential component of RPD3S) or Sds3 (a specific and essential component of RPD3L) (Carrozza *et al*, 2005b). While the absence of Rco1 had virtually no effect, deletion of the RPD3L components dramatically alleviated the repression of *Ribi*/*RP* genes that would otherwise be observed upon Sch9 inhibition (Figure 2A; Supplementary Figure S2A and B). These observations strongly suggest that Stb3, Dot6 and Tod6 repress transcription of the *Ribi* and *RP* regulons via RPD3L.

Effects of Stb3, Dot6 and Tod6 on cell growth and cell size

Cells in which *Ribi* gene expression is compromised exhibit a reduced growth rate and a small cell size (Jorgensen *et al*, 2004). The absence of Sch9 activity in particular causes

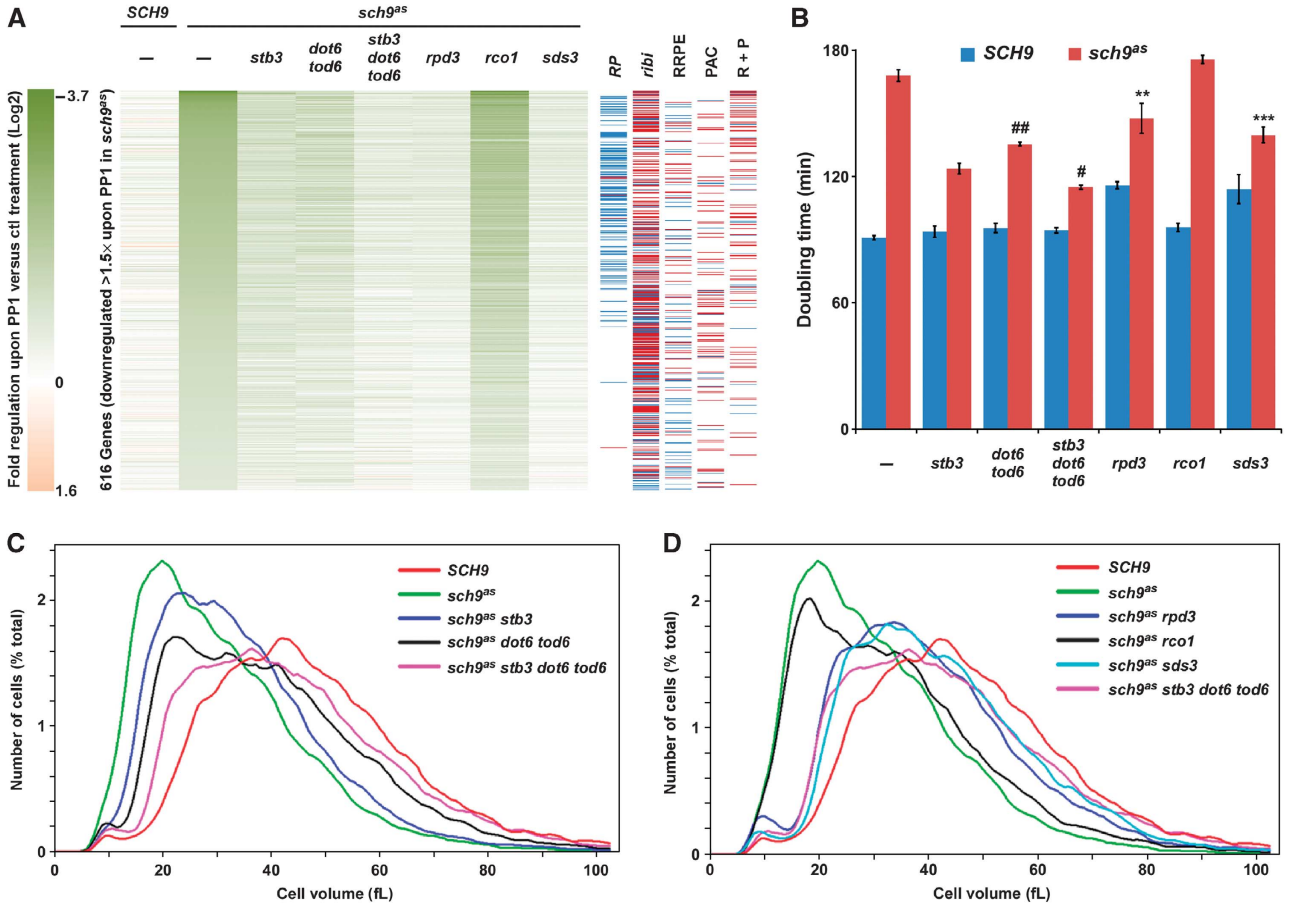

Figure 2 Sch9 regulates cell growth via Stb3, Dot6, Tod6 and RPD3L. (**A**) Regulation of *Ribi* and *RP* transcription. Strains of the indicated genotype were grown to exponential phase in YPD at 30°C, treated for 30 min with 1NM-PP1 (PP1) or drug vehicle, followed by determination of mRNA-Seq transcriptome profiles. All genes downregulated >1.5-fold by 1NM-PP1 versus drug vehicle in the $sch9^{as}$ strain are shown, as sorted by magnitude of change. In the right panels, genes belonging to the *Ribi* or *RP* regulons or whose promoters contain RRPE or PAC promoter elements or both (R + P) (Jorgensen and Tyers, 2004) are indicated with blue dashes if derepressed preferentially by *STB3* deletion or red dashes if derepressed preferentially by *DOT6/TOD6* deletion. (**B**) Regulation of growth rate. *SCH9* and $sch9^{as}$ strains harbouring the indicated gene deletions were grown to exponential phase at 30°C in YPD in the presence of 1NM-PP1 and doubling times calculated from quantitative growth curves. Growth rate effects were recapitulated in spot assays; the phenotypes of the *stb3*Δ and *dot6*Δ *tod6*Δ strains were confirmed by complementation with plasmid-encoded wild-type alleles (Supplementary Figure S3A and B). Data are means of three independent experiments ± s.d. $^{**}P<0.01$; $^{***}P<0.001$ versus $sch9^{as}$. $^{\#}P<0.05$; $^{\#\#}P<0.01$ versus $sch9^{as}$*stb3*Δ. (**C**, **D**) Regulation of cell size. Strains of the indicated genotypes were grown as in (**B**) and cell size distributions determined on a Z2 Coulter counter. Size profiles are shown in two separate panels with the same scales for clarity. Corresponding $SCH9^{wt}$ control distributions were also determined (Supplementary Figure S3B and C; see Supplementary Table S2 for all quantitative size parameters).

a severe small size (Whi) phenotype and a marked growth defect (Jorgensen *et al*, 2002). We determined if these phenotypes are mediated via Stb3, Dot6, Tod6 and the RPD3L complex. Our wild-type strain had a doubling time (t_d) of ~90 min and a mode cell volume of 41 fL (Figure 2B–D; Supplementary Figure S3C and D; Supplementary Table S2); inhibition of an $sch9^{as}$ strain with 1NM-PP1 increased the doubling time to about 170 min and decreased mode cell volume to about 20 fL. This decreased cell size is attributable to a reduced critical size threshold at the point of commitment to division (Start), as estimated by the half height value of the daughter cell (left hand) side of the size distribution (half height daughter size for wild type = 24 fL and for $sch9^{as}$ with 1NM-PP1 = 12 fL). Deletion of *STB3* in the $sch9^{as}$ strain strongly suppressed the slow growth phenotype (t_d = 125 min) and partially suppressed the cell size defect (daughter size = 14 fL). Importantly, the *stb3*Δ strain itself was wild type in size (Supplementary Figure S3C), thereby demonstrating that the size rescue effect was epistatic rather than additive. Deletion of *DOT6* and *TOD6* more potently rescued the size defect (daughter size = 17 fL) but suppressed the slow growth phenotype to a lesser extent (t_d = 135 min). As the *dot6*Δ *tod6*Δ strain had a somewhat larger size than wild type (Supplementary Figure S3C), the increase in size was more pronounced in the $sch9^{as}$ background (42% increase in $sch9^{as}$ versus 23% increase in wild type), again consistent with an epistatic interaction. Combined deletion of the three genes further suppressed both phenotypes (t_d = 115 min; daughter size = 20 fL), consistent with the observed synthetic transcriptional effects. As predicted, deletion of either *RPD3* or *SDS3* fully recapitulated the size suppression by the deletion of *STB3*, *DOT6* and *TOD6* (daughter sizes = 20 and 22 fL, respectively). However, the *rpd3*Δ and *sds3*Δ mutations only slightly rescued the growth rate phenotype of $sch9^{as}$ cells (t_d = 145 and 140 min, respectively), in part due to an Sch9-independent slow growth phenotype (t_d = 115 min

in both strains). Deletion of the RPD3S subunit, *RCO1*, did not suppress either *sch9* phenotype ($t_d = 175$ min doubling time; daughter size = 12 fL). Independent flow cytometric determination of total cell protein content confirmed that the suppression of cell size defects was due to differences in biomass and not due to increased vacuolarization (Supplementary Figure S3E). We note that even the strongest size suppression effects did not fully restore size to wild type, suggesting that additional Sch9 effectors likely influence the size threshold. Collectively, these results indicate that Stb3 and Dot6/Tod6 function in concert with the RPD3L complex to regulate growth rate and cell size.

Sch9 regulates RNA polymerase I and III via Stb3, Dot6 and Tod6

TORC1/Sch9 regulates rRNA transcription by RNAPI through an Rrn3-independent pathway (Huber *et al*, 2009; Wei and Zheng, 2009; Philippi *et al*, 2010); in addition, Sch9 regulates rRNA processing (Huber *et al*, 2009). Since the *Ribi* regulon contains many genes involved in rRNA transcription and processing, and since RPs appear to have indirect roles in these processes (Reiter *et al*, 2011), we wondered if Sch9 indirectly promotes rRNA transcription and/or processing via the *Ribi* and *RP* regulons. We assayed RNAPI transcription by Miller chromatin spreads (Figure 3A and B) and found that Sch9 inhibition reduced the number of polymerases per 35S rRNA gene by >60%. This defect was partially suppressed by the disruption of *STB3*, *DOT6/TOD6* or *RPD3*. We then performed metabolic pulse-labelling experiments with ^{3}H-uracil to examine effects on rRNA synthesis and processing (Huber *et al*, 2009). Sch9 inhibition reduced the incorporation of radioactivity into rRNA and caused a defect in 27S–25S and 20S–18S rRNA maturation (Figure 3C). Disruption of *STB3* partially rescued both effects, while disruption of *DOT6* and *TOD6* resulted in a relative accumulation of 27S and 20S species, suggesting that rRNA transcription was partially restored but that the processing phenotype was not. Again, deletion of all three transcription factors, or deletion of *RPD3* alone, further rescued the rRNA transcription and processing defects. Interestingly, the downregulation of

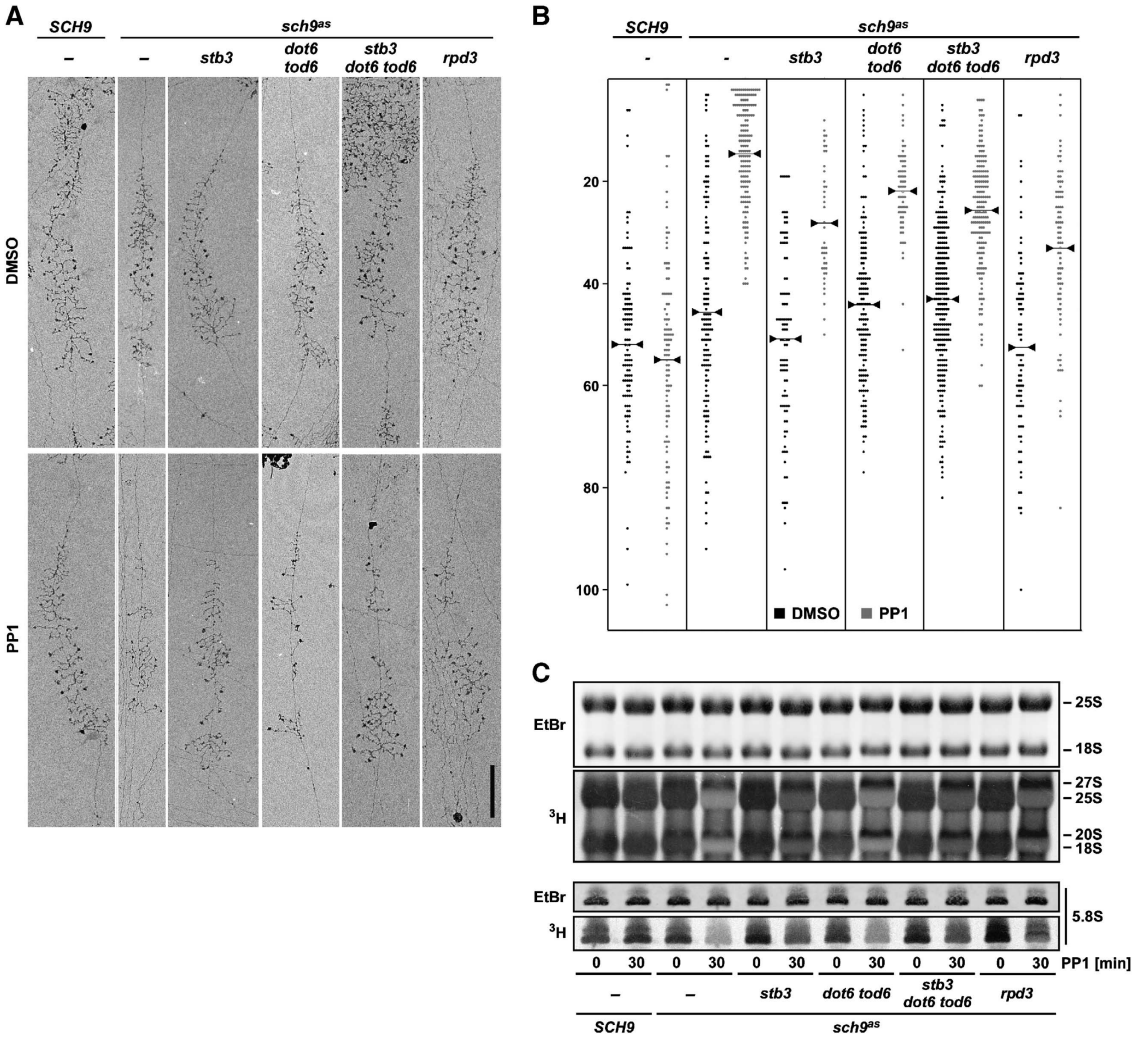

Figure 3 Stb3, Dot6 and Tod6 regulate RNA Pol I transcription initiation and rRNA processing. (**A**, **B**) Miller chromatin spreads were prepared from the indicated strains treated for 30 min with 1NM-PP1 or DMSO. (**A**) Representative electron micrographs of transcribed rDNA genes in Miller spreads. (**B**) The number of polymerases of each active *rDNA* repeat was determined and plotted. Averages are marked for each group with a line bounded by triangles. (**C**) RNA synthesis in the indicated strains following DMSO or 1NM-PP1 treatment was determined by metabolic pulse labelling with ^{3}H-uracil. Total RNA loaded was visualized by staining with ethidium bromide (EtBr). Mature rRNA (25S and 18S) and pre-rRNA (27S and 20S) species are indicated.

5S rRNA and tRNA production upon Sch9 inhibition was also partially ameliorated by elimination of *STB3*, *DOT6/TOD6* or RPD3L function (Supplementary Figure S4). These findings reveal that Sch9 regulates both rRNA transcription/processing and tRNA synthesis via the same cohort of Rpd3-associated effectors that govern *Ribi* and *RP* gene expression.

Phosphorylation of Stb3, Dot6 and Tod6 regulates their repressive activities

Given that Stb3, Dot6 and Tod6 phosphorylation negatively correlated with their repressive activity (Figures 1A–C and 2A), we mutated the known Sch9 sites in each protein and assessed the phenotypic consequences. Five sites in Stb3 match the R[R/K]x[S/T] Sch9/PKA consensus motif, three of which (S254, S285 and S286) have been reported in phosphoproteomic profiles (Chi *et al*, 2007; Bodenmiller *et al*, 2008; Huber *et al*, 2009; Soulard *et al*, 2010; Stark *et al*, 2010). Replacing all three sites with non-phosphorylatable Ala residues yielded a variant ($Stb3^{3A}$) that was not recognized by a phosphospecific antibody *in vivo* (Supplementary Figure S1A and B). Overexpression of $STB3^{3A}$ but not wild-type *STB3* impaired cell growth and decreased *RP* gene expression (Figure 4A; Supplementary Figure S5A). While this *RP* defect was partially suppressed in an *sds3*Δ strain (Supplementary Figure S5A and B), consistent with a previous report (Liko *et al*, 2010), the toxicity of $STB3^{3A}$ overexpression was not suppressed by disruption of RPD3L function (Figure 4A). Unlike previous studies (Liko *et al*, 2010), we detected only marginal suppression of $STB3^{3A}$ toxicity upon disruption of the *HOS2* histone deacetylase gene. Furthermore, deletion of *HOS2* suppressed neither the defects in growth rate nor *Ribi* or *RP* gene expression of an $sch9^{as}$ strain in our genetic background

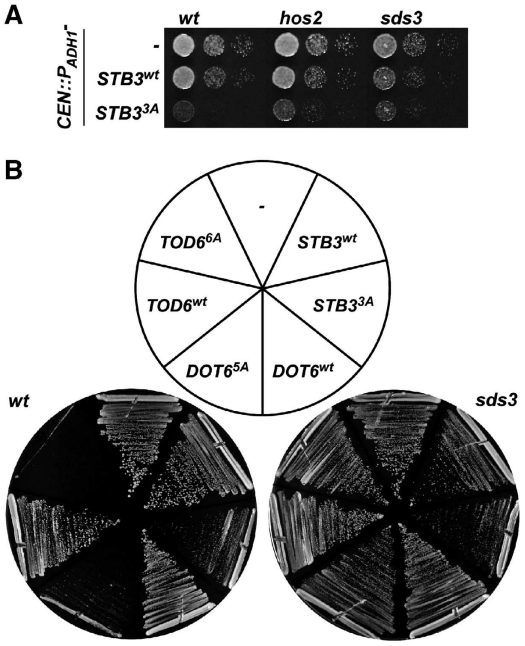

Figure 4 Stb3, Dot6 and Tod6 phosphorylation regulates their activity *in vivo*. (**A**, **B**) The indicated strains were transformed with *CEN*-based plasmids expressing the indicated alleles of *STB3*, *DOT6* or *TOD6* from the strong constitutive *ADH1* promoter. Cells were then plated in 10-fold dilution series (**A**) or restruck (**B**) onto selective synthetic medium and grown for 3 days at 30°C.

(Supplementary Figure S5C and D). These negative results are consistent with the previous reports that Hos2 has virtually no influence on the broad transcriptional profile elicited by rapamycin (Humphrey *et al*, 2004).

We had previously mapped five phosphorylation sites in Dot6 and six sites in Tod6, all of which corresponded to the R[R/K]x[S/T] consensus except for S247 in Dot6, which still fits a minimal RxxS consensus (Huber *et al*, 2009). Dot6 and Tod6 variants in which these sites were substituted with Ala residues ($Dot6^{5A}$ and $Tod6^{6A}$) were not as robustly phosphorylated by Sch9 in an *in vitro* kinase assay (Figure 1E and F). Overexpression of $DOT6^{5A}$ and $TOD6^{6A}$, but not wild-type alleles caused a severe slow growth phenotype that was largely suppressed by deletion of *SDS3* (Figure 4B). Because of the severity of the $DOT6^{5A}$- and $TOD6^{6A}$-associated growth phenotypes, we verified this result by conditional expression of each allele from the *GAL1* promoter (Supplementary Figure S6A). On galactose medium, overexpression of the non-phosphorylatable Dot6 and Tod6 variants again caused a strong growth phenotype, which was suppressed by deletion of *RPD3* or *SDS3* but not *RCO1*. Similar results were also obtained with a doxycycline-inducible system (Supplementary Figure S6B and C). In agreement with the growth defects, *Ribi* and *RP* gene transcription was strongly repressed upon overexpression of the non-phosphorylatable variants of Dot6 and Tod6 compared with their wild-type counterparts, and was restored upon disruption of RPD3L function (Supplementary Figure S6D). Collectively, these data demonstrate that Sch9-dependent phosphorylation antagonizes the repressive functions of Stb3, Dot6 and Tod6.

Negative feedback regulation of Tod6 and homeostatic control of Ribi/RP genes

In several assays for Tod6 phosphorylation, we noticed that Tod6 levels were decreased when the protein was hypophosphorylated (Figure 1C). Tod6–5HA levels were diminished in a $sch9^{as}$ strain (the $sch9^{as}$ allele is slightly hypomorphic; Jorgensen *et al*, 2004) and further decreased upon treatment with 1NM-PP1 (Figure 5A). Similarly, the $Tod6^{6A}$–5HA phosphosite mutant was less abundant as compared with the wild-type protein (Figure 5B and C). In part, this effect was due to diminished expression of $TOD6^{6A}$*–5HA* as compared with wild-type *TOD6–5HA* mRNA (Figure 5C). The reduced abundance of the $TOD6^{6A}$*–5HA* transcript levels was not due to *cis* destabilization effects because expression of this allele also decreased the endogenous *TOD6* transcript (Figure 5D). These observations are consistent with the fact that *TOD6* is part of the *Ribi* regulon (Wade *et al*, 2006), with the down-regulation of *TOD6* upon Sch9 inhibition (Supplementary File F1), with the regulated recruitment of RPD3L to the *TOD6* promoter (see below) and with the specific effects of *TOD6* on *Ribi* gene expression (Supplementary Figure S7). In addition, the $Tod6^{6A}$–5HA protein/mRNA ratio was significantly decreased compared with the wild-type ratio (Figure 5C), suggesting that Tod6 dephosphorylation may destabilize the protein. We were unable to directly test this hypothesis because the effects of both translational inhibitors and nutrient shifts on Sch9 activity (Urban *et al*, 2007) would confound interpretation of wild-type Tod6 half-life data. We conclude that Tod6 negatively represses its own transcription in a manner that is antagonized by Sch9-dependent phosphorylation, and that Tod6 phosphorylation may promote its

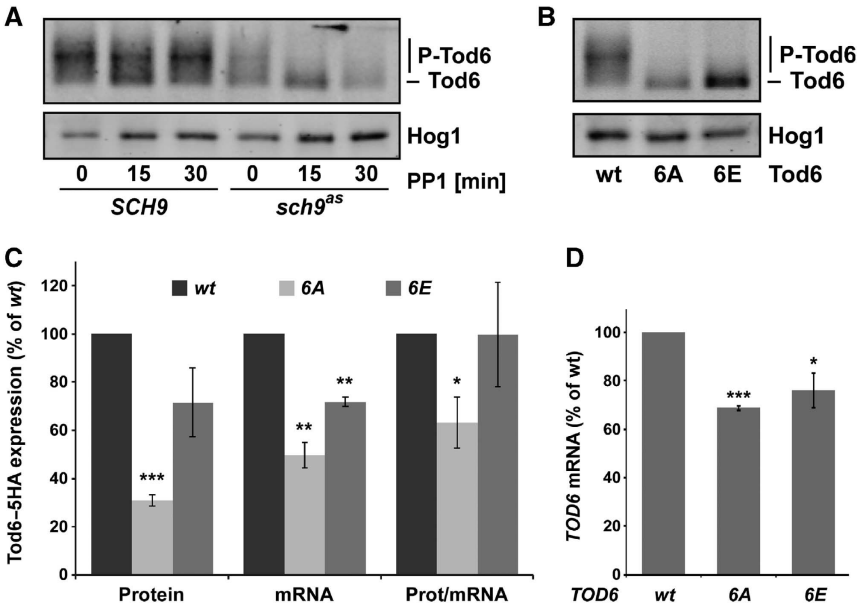

Figure 5 Regulation of Tod6 expression level and protein abundance. (**A**) *SCH9* and *sch9*^{as} cells expressing Tod6–5HA were grown in YPD at 30°C and subjected to 300 nM 1NM-PP1 treatment as indicated. Proteins were extracted under denaturing conditions and analysed by western blot against the HA epitope; an antibody specific to the Hog1 protein served as loading control. (**B**) Strains expressing the indicated TOD6–5HA alleles were grown to exponential phase in SC-URA at 30°C and proteins were extracted and analysed as in (**A**). (**C**) Quantification of Tod6–5HA versus Hog1 abundance shown in (**B**) and two other independent experiments. Quantification of TOD6–5HA versus ACT1 mRNA expression was determined from total RNA extracts from the same strains as in (**B**). The ratio of Tod6–5HA protein to TOD6–HA mRNA was calculated from these values and shown as mean ± s.d. of three independent experiments. (**D**) Endogenous TOD6 versus ACT1 expression levels for the same RNA extracts shown in (**C**). Values are mean ± s.d. of three independent experiments. $*P<0.05$; $**P>0.01$; $***P<0.001$ versus wild-type control.

stability. Altogether these data suggest that Tod6 is part of a homeostatic control mechanism of *Ribi* gene transcription involving negative feedback loops on its expression and possibly stability.

RPD3L is recruited to Ribi/RP gene promoters by Stb3, Dot6 and Tod6

As Stb3, Dot6 and Tod6 each interact with RPD3L subunits (Kasten and Stillman, 1997; Shevchenko *et al*, 2008), we hypothesized that these factors may recruit the RPD3L deacetylase complex to *RP* and *Ribi* promoter DNA. Coimmunoprecipitation experiments confirmed that each factor interacted with RPD3L and, somewhat surprisingly, revealed that the interactions were not sensitive to Sch9 activity (Supplementary Figure S8A and B). We next asked if RPD3L was recruited to the relevant promoter regions upon Sch9 inhibition and whether this recruitment was dependent on Stb3 and/or Dot6/Tod6. We used a TAP-tagged version of Sds3 for chromatin immunoprecipitation followed by high-throughput sequencing (ChIP-Seq). RPD3L-associated sequences were detected using the MACS algorithm and mapped to downstream ORFs on both DNA strands (Supplementary File F2). In comparison to a mock ChIP signal obtained with untagged Sds3, 875 peaks were mapped to the promoters of 943 genes in the Sds3–TAP immunoprecipitations. Of these, 223 peaks in 271 promoters were upregulated >1.5-fold in an *sch9*^{as} strain treated with 1NM-PP1 compared with the untagged control strain (Figure 6A; Supplementary Figure S9A and B; Supplementary Table S3). Analyses of these RPD3L ChIP-Seq profiles revealed that *RP* promoters were highly enriched ($P<10^{-9}$) and that *Ribi* promoters were enriched to a lesser extent ($P<0.01$). Assessment of the genetic dependencies of these profiles revealed that RPD3L peaks that depended on Stb3 were highly enriched in *RP* gene promoters ($P<10^{-12}$), whereas the majority of RPD3L peaks in *Ribi* gene promoters were preferentially but not exclusively dependent on Dot6 and Tod6 (20 *Ribi* genes; $P<0.05$). The Stb3- versus Dot6/Tod6-dependent RPD3L recruitment to *RP* and *Ribi* gene promoters was significantly correlated with the Stb3- versus Dot6/Tod6-dependent regulation of *RP* and *Ribi* genes by Sch9 (Supplementary Figure S10; $P<10^{-4}$). In the absence of all three repressive transcription factors, the RPD3L peaks at the promoters of both *RP* and *Ribi* promoters were equivalent to those in an *SCH9* control strain (Figure 6A; Supplementary Figure S9C). These ChIP-Seq data were confirmed by conventional ChIP–qPCR experiments for selected *Ribi* and *RP* genes (Supplementary Figure S11A). Overall, the influence of *STB3* and *DOT6/TOD6* deletions on RPD3L recruitment closely paralleled their effects on transcriptome profiles (Figure 2A; Supplementary Table S1). The combination of ChIP-Seq, transcriptome profiling and protein–protein interaction data strongly support a model whereby Stb3, Dot6 and Tod6 serve to physically recruit the RPD3L histone deacetylase complex upstream of *Ribi* and *RP* genes.

Our finding that RPD3L was recruited to *RP* gene promoters almost exclusively by Stb3 was somewhat puzzling given that Stb3 was identified as a sequence-specific partner for the RRPE element that is strongly enriched upstream of *Ribi* and not *RP* genes (Liko *et al*, 2007). We, therefore, located Stb3 interaction regions in the genome by repeating the ChIP-Seq analyses with an Stb3–TAP fusion protein. Compared with RPD3L, Stb3 showed strong occupancy at fewer loci, almost

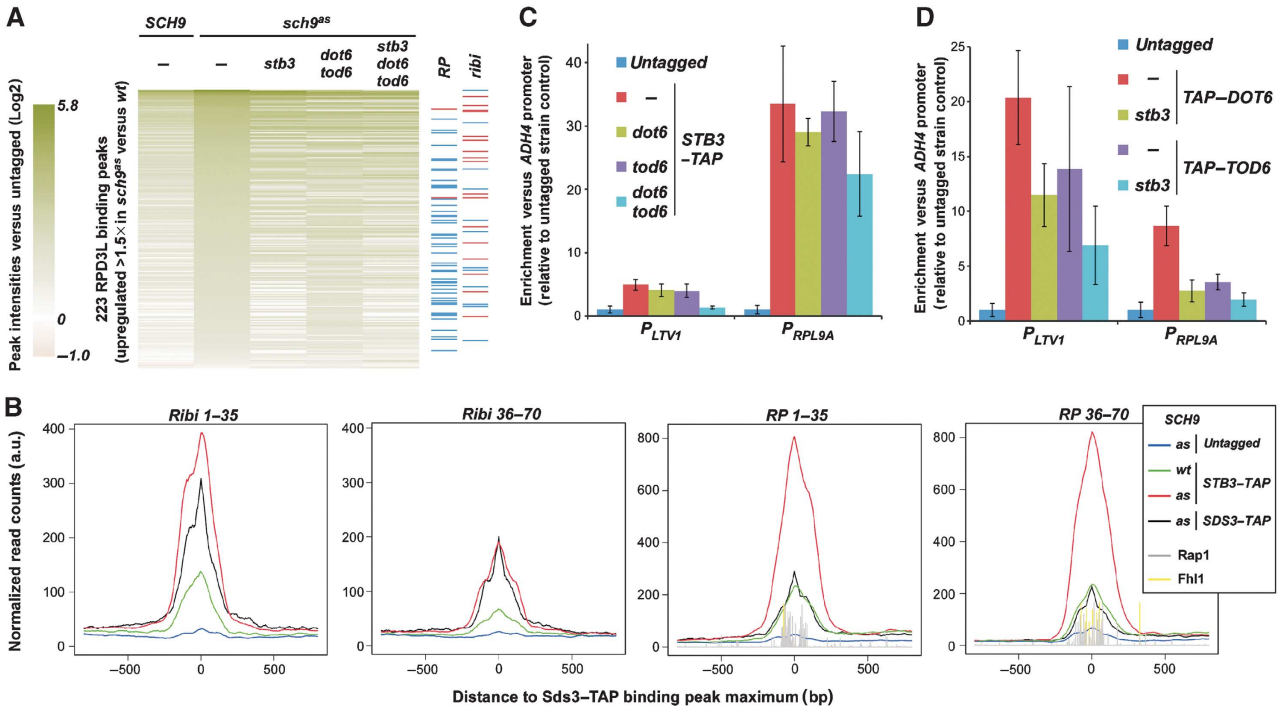

Figure 6 RPD3L recruitment to *Ribi* and *RP* promoters upon Sch9 inhibition in a Stb3- and Dot6/Tod6-dependent manner. (**A**) Strains of the indicated genotype expressing an Sds3–TAP fusion protein were grown exponentially in YPD at 30°C and treated with 300 nM 1NM-PP1 for 20 min followed by fixation, chromatin extraction and ChIP-Seq analysis. Sds3 (RPD3L)-associated sequences were detected by comparing read counts from the *sch9^{as}SDS3–TAP* strain to an *sch9^{as}* (untagged) mock control using the MACS algorithm. Peak intensities were calculated in all conditions at these loci (Supplementary File F2) and normalized to the untagged control counts. Peaks showing an upregulation >1.5-fold in the *sch9^{as}* strain compared with wild type are shown as sorted by magnitude of change. In the right panels, peaks mapping to *Ribi* or *RP* gene promoters are indicated with blue dashes if upregulation upon Sch9 inhibition was preferentially suppressed by *STB3* deletion, or with red dashes if upregulation upon Sch9 inhibition was preferentially suppressed by *DOT6/TOD6* deletion. (**B**) Strains of the indicated genotype expressing an Stb3–TAP fusion protein or untagged Stb3 (mock control) were grown, treated and processed for ChIP-Seq analysis as in (**A**). In all, 70 peaks of Sds3–TAP (RPD3L) binding mapping to *Ribi* gene promoters were sorted according to their score (Supplementary File F2) and divided into two sets (*Ribi* 1–35 and 36–70). Each set of peaks were aligned according to their maxima, summed and plotted for each condition (black line; left panels). Total read counts mapping to the aligned loci in the Stb3–TAP ChIP-Seq analyses (red and green) and their mock control (blue) were also plotted. A similar analysis for peaks mapping to *RP* gene promoters was performed (right panels). The relative position of Rap1 (grey) and Fhl1 (yellow) binding sites in these promoters was evaluated by scoring each loci using previously published position weight matrices of the corresponding motifs (Harbison *et al*, 2004). (**C**, **D**) Stb3 and Dot6/Tod6 cooperate to bind upstream of *Ribi* genes. *sch9^{as}* strains bearing the indicated gene deletions and expressing the indicated TAP-tagged proteins were grown exponentially in YPD at 30°C and treated with 300 nM 1NM-PP1 for 20 min. Cells were then fixed and processed for ChIP–qPCR analysis for the indicated loci. Data are shown as mean ± s.d. of four (**C**) and three (**D**) independent experiments.

all of which were upregulated upon Sch9 inhibition (635 out of 636 peaks) and coincident with the Sch9-sensitive RPD3L peaks in *Ribi* and *RP* promoters (Figure 6B; Supplementary Figure S9A and B). The Stb3 ChIP-Seq data were also confirmed by ChIP–qPCR for selected *Ribi* and *RP* genes (Supplementary Figure S11B). ChIP–qPCR also revealed that Dot6 interactions with the *LTV1* and *NOP14* promoters were strongly upregulated upon Sch9 inhibition (Supplementary Figure S11C). Tod6 also occupies these loci, but was not overtly responsive to Sch9 inhibition. This apparent lack of regulation should be interpreted with caution, however, as Tod6 levels are markedly lower in a *sch9^{as}* strain and decrease further upon 1NM-PP1 treatment (Figure 5A; Supplementary Figure S8B). In contrast to Stb3, we observed that both Dot6 and Tod6 preferentially occupied *Ribi* gene promoters as the ChIP–qPCR upstream of *RP* genes was only slightly above background (Supplementary Figure S11C).

As Stb3, Dot6 and Tod6 each showed detectable binding upstream of *Ribi* and *RP* genes, we asked whether their recruitment was interdependent. We thus examined the interactions of Stb3–TAP at the *LTV1* (*Ribi*) and *RPL9A* (*RP*) promoters in a 1NM-PP1-treated *sch9^{as}* strain upon *DOT6* and/or *TOD6* deletion. The single deletions had little or no impact on the Stb3 signal at either loci. In the *dot6*Δ *tod6*Δ background, however, Stb3 recruitment upstream of *LTV1* was reduced to background levels, whereas its interaction with the *RPL9A* promoter was only slightly affected (Figure 6C). We then asked whether Dot6/Tod6 recruitment to these loci was dependent upon *STB3*. The interaction of both Dot6 and Tod6 was partially impaired at the *LTV1* promoter and completely absent at the *RPL9A* promoter in the *stb3*Δ background (Figure 6D). These ChIP data suggest that upon Sch9 inhibition, Stb3 and Dot6/Tod6 bind upstream of *Ribi* genes in a cooperative manner to recruit the RPD3L histone deacetylase complex, while RPD3L tethering to *RP* gene promoters depends mainly on Stb3, with only a minor influence of Dot6/Tod6. These observations consistently correlate with the relative effects of Stb3, Dot6 and Tod6 on the transcriptional regulation of *Ribi* and *RP* genes.

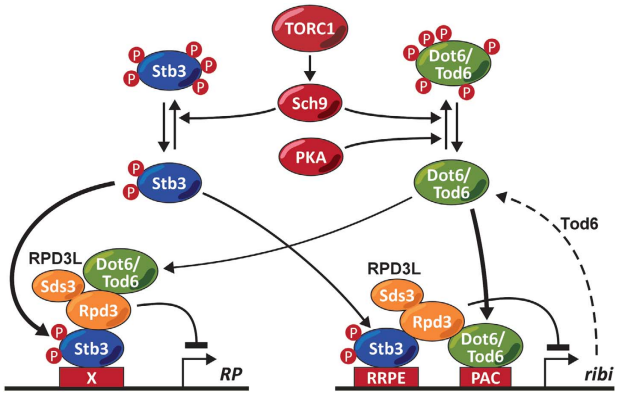

Figure 7 Sch9 regulates ribosome biogenesis via Stb3, Dot6 and Tod6 and the histone deacetylase complex RPD3L. Sch9 directly phosphorylates the transcription repressors Stb3, Dot6 and Tod6 to antagonize their ability to recruit the RPD3L histone deacetylase to *RP* and *ribi* promoters. The thicker arrows indicate that Stb3 primarily mediates suppression of *RP* genes while Dot6/Tod6 primarily mediate suppression of *ribi* genes. The dashed arrow labelled Tod6 is included to highlight the fact that *TOD6* belongs to the *ribi* regulon and thus participates in a feedback loop to maintain homeostasis of *ribi* gene expression. Please see text for further details.

Discussion

We show here that the three transcriptional repressors, Stb3, Dot6 and Tod6, are directly phosphorylated by the Sch9 kinase to allow physiological regulation of the *Ribi* and *RP* regulons in response to TORC1-mediated nutrient signals. These observations build on our previous analysis of the rapamycin-sensitive phosphoproteome (Huber *et al*, 2009), and on previous genetic data that implicate Stb3, Dot6 and Tod6 in the regulation of *Ribi* and *RP* genes downstream of TORC1/Sch9 and PKA (Lippman and Broach, 2009; Liko *et al*, 2010). Our analysis shows that Sch9-dependent regulation of *RP* gene transcription is mediated primarily by Stb3 whereas Sch9-dependent regulation of *Ribi* gene transcription is mediated by Dot6, Tod6 and, to a lesser extent, Stb3. We provide a mechanistic basis for the repressive activity of the three transcription factors, namely that the histone deacetylase complex RPD3L is recruited to *Ribi* and *RP* gene promoters upon Sch9 inhibition in an Stb3- and Dot6/Tod6-dependent manner. A model that encapsulates these results is presented in Figure 7.

Several observations suggest that RPD3L recruitment is the primary mechanism by which these three transcription factors repress *Ribi* and *RP* transcription: (i) Stb3, Dot6 and Tod6 interact physically with RPD3L (Supplementary Figure S8A and B) (Kasten and Stillman, 1997; Shevchenko *et al*, 2008); (ii) disruption of RPD3L phenocopies the derepression of *Ribi* and *RP* genes caused by deletion of *STB3*, *DOT6* and *TOD6* when Sch9 is inhibited (Figures 2A–C and 3A and B; Supplementary Figure S2A); (iii) the relative dependency on Stb3 versus Dot6/Tod6 for RPD3L recruitment to *Ribi* and *RP* gene promoters correlates with the transcriptional regulation of these regulons (Figures 2A and 6A; Supplementary Figure S10); and (iv) overexpression of non-phosphorylatable Dot6 and Tod6 variants impairs growth in an RPD3L-dependent manner (Figure 4B; Supplementary Figure S6A–D).

Recently, it has been suggested that Stb3 acts by recruiting the Hos2 histone deacetylase to repress transcription because deletion of *HOS2* but not *RPD3* suppressed the growth defect caused by Stb3 overexpression (Liko *et al*, 2010). However, in our strain background, deletion of *HOS2* does not suppress the severe growth phenotype observed upon $Stb3^{3A}$ overexpression (Figure 4A), nor does it alleviate the repression of Stb3-dependent *Ribi* and *RP* genes observed upon inhibition of Sch9 (Supplementary Figure S6B). In agreement with our data, two independent studies showed that Rpd3, but not Hos2, couples TORC1 signals to *Ribi* and *RP* genes (Rohde and Cardenas, 2003; Humphrey *et al*, 2004). Nevertheless, it is puzzling that RPD3L disruption did not suppress the $Stb3^{3A}$-induced slow growth phenotype in our strain background (Figure 4B). Although several explanations can be envisioned, at present we favour the hypothesis that $Stb3^{3A}$ represses *Ribi/RP* transcription not only via recruitment of RPD3L but also by displacing and/or otherwise interfering with Fhl1/Rap1 function. This hypothesis is based on our ChIP-Seq profiles, which indicate that RPD3L and Stb3 chromatin binding sites are very close to, if not coincident with, Fhl1 and Rap1 binding sites (Figure 6B). This observation suggests that $Stb3^{3A}$ could effectively interfere with Fhl1/Rap1 functions, for example by antagonizing recruitment of the critical transcriptional activator Ifh1. The predictions of this model remain to be tested.

How does Sch9 regulate Stb3, Dot6 and Tod6? Sch9 was previously shown to antagonize the nuclear accumulation of Stb3 (Liko *et al*, 2010). Notably, unlike many other regulated transcription factor complexes, we did not detect any change in Stb3 affinity for RPD3L upon Sch9 inhibition (Supplementary Figure S8A). Nucleocytoplasmic shuttling and/or the affinity of its association with chromatin are other potential points of Stb3 regulation. In contrast to Stb3, Dot6 and Tod6 localize to the nucleus in rapidly growing cells and this localization is not apparently regulated by Sch9 (data not shown). Similar to Stb3, the interactions between Dot6 or Tod6 and RPD3L also did not seem to be altered upon Sch9 inhibition (Supplementary Figure S9B). Thus, we hypothesize that Sch9-dependent phosphorylation regulates the ability of Dot6 and Tod6 to interact with chromatin. As the recruitment of Stb3 and Dot6/Tod6 appears to be interdependent (Figure 6C and D), these factors may physically interact at chromatin and/or alter the local chromatin environment to facilitate mutual interactions.

Delineating the precise roles of individual phosphorylation events in Stb3, Dot6 and Tod6 will be a challenge. Large-scale mass spectrometric studies (Chi *et al*, 2007; Bodenmiller *et al*, 2008; Huber *et al*, 2009; Soulard *et al*, 2010; Stark *et al*, 2010) suggest that these factors are phosphorylated on >50 sites in total. Furthermore, although we could not confirm previous reports that Stb3 phosphorylation is regulated by PKA (Budovskaya *et al*, 2005), we did confirm that Dot6 and Tod6 phosphorylation is regulated downstream of PKA (Figure 1B and C) (Deminoff *et al*, 2006). Thus, like Maf1 (Huber *et al*, 2009; Lee *et al*, 2009; Wei and Zheng, 2009; Ramachandran and Herman, 2011), Dot6 and Tod6 represent a convergence point for growth regulation mediated by TORC1 and PKA.

Previously, we showed that Sch9 regulates RNAPI and III transcription (Huber *et al*, 2009). Here, we demonstrate that at least part of this regulation is mediated on a relatively short timescale by Stb3 and Dot6/Tod6 (30 min Sch9 inhibition; Figure 3A–C). As we have been unable to detect binding

of any of these transcription factors to the rDNA locus (Supplementary Figure S11A–C), we speculate that this regulation occurs indirectly via the expression of *Ribi* genes, many of which encode factors involved in RNAPI/III transcription (Jorgensen *et al*, 2004; Wade *et al*, 2006). However, as deletion of *STB3*, *DOT6* and *TOD6* only partially blocks the reduction in rRNA transcription observed upon Sch9 inhibition, it is likely that another target of Sch9 involved in RNAPI regulation remains to be identified.

We also found that Stb3 influences rRNA processing. This observation was not in itself surprising as many *Ribi* gene products are implicated in this process (Jorgensen *et al*, 2004; Wade *et al*, 2006). However, the result that Stb3, which regulates primarily *RP* rather than *Ribi* transcription, seems to have an exclusive role in regulating 27S–25S and 20S–18S rRNA processing (Figure 3B) was unexpected. We note that RP synthesis and incorporation into the 40S and 60S ribosomal subunits is coupled with the maturation of the corresponding rRNAs (Ferreira-Cerca *et al*, 2005; Poll *et al*, 2009; Reiter *et al*, 2011).

We have shown previously that Ribi influences not only growth rate but also the critical cell size threshold (Jorgensen *et al*, 2002, 2004). This effect of Ribi on cell size is independent from effects on protein synthesis *per se* (Jorgensen *et al*, 2004). We found that Stb3 affects the rate of cell growth more potently than Dot6/Tod6 (Figure 2B), consistent with the predominant effects of Stb3 on *RP* gene expression. In contrast, Dot6/Tod6 have a greater influence on cell size than Stb3 (Figure 2C), also consistent with their primary effect on the *Ribi* regulon. As deletion of *STB3*, *DOT6* and *TOD6* did not completely alleviate the small size caused by Sch9 inhibition, we again infer the existence of other Sch9 effectors for cell size. These observations will serve as a starting point to further dissect how the Ribi machinery communicates growth potential to the cell division machinery at Start.

Finally, our studies have uncovered an additional feedback loop in ribosome biogenesis, namely the autoregulation of Tod6 activity in the control of *Ribi* gene expression (Figure 5C and D; Supplementary Figures S6 and S7). This negative transcriptional feedback mechanism in principle imposes homeostatic control on Ribi (Supplementary Figure S6), and may act in concert with previously reported signalling feedback loops on Sch9 and Sfp1 (Jorgensen *et al*, 2004; Mnaimneh *et al*, 2004; Lempiainen *et al*, 2009). Understanding the complex interactions of these feedback loops as the primary means of establishing homeostatic control of ribosome biogenesis will be an intriguing and challenging area of future research.

Materials and methods

Yeast strains and growth assays

S. cerevisiae strains and plasmids are described in Supplementary Tables S4 and S5, respectively. Strains were constructed according to the standard protocols. Unless specified otherwise, rapamycin was used at 200 nM (from a 1-mM stock solution in 90% ethanol, 10% Tween-20), and 1NM-PP1 at 300 nM (from 1 mM or 10 mM stocks in DMSO).

For growth rate assays, cells growing exponentially were diluted in the indicated media to an OD_{600} of $\leqslant 0.025$ and 200 μl aliquots were dispensed in transparent 96-well plates. Wells were loaded with medium without cells to serve as reference. The plates were incubated at 30°C and OD_{600} was measured every 15 min for each well in a Sunrise microplate reader (Tecan, Switzerland). Reference values measured from medium alone were subtracted from all measurements. Doubling times were calculated from the slopes of linear regressions on the OD_{600} after Log2 transformation as a function of time once the cultures reached an OD_{600} of 0.2.

Cell size assays were performed on exponential phase cultures using a Z2 Coulter counter, as described previously (Jorgensen *et al*, 2002).

Denaturing protein extraction and immunoprecipitation

Denaturing protein extracts were performed using the TCA-Urea method as described previously (Urban *et al*, 2007). For immunoprecipitation, denatured extracts were diluted 10-fold in native lysis buffer (PBS 10% glycerol 0.5% Tween-20) supplemented with 10 mM NaF, 10 mM *p*-nitrophenylphosphate, 10 mM $Na_2P_2O_4$, 10 mM β-glycerophosphate, 1 × Roche protease inhibitor cocktail and 1 mM PMSF and cleared by centrifugation at full speed in a microcentrifuge. A total of 10 μl anti-HA sepharose beads was added to the supernatants, incubated for 2 h at 4°C and washed 3 × with native lysis buffer. Immunoprecipitated proteins were analysed by western blotting with anti-HA and anti R[R/K]x[S/T]* (Cell Signaling) antibodies.

Sch9 kinase assays

TAP–Sch9 variants were expressed and purified as described previously (Huber *et al*, 2009) except that magnetic beads coated with rabbit IgG (Invitrogen) were used instead of glutathione-coated sepharose beads and the purified kinase was not eluted from the beads. Recombinant GST, GST–Stb3, GST–Dot6 and GST–Tod6 fusion protein variants were expressed using the pGEX6P1 system as described previously (Huber *et al*, 2009) except that the proteins were eluted using PBS 20% glycerol 0.5% Tween-20 supplemented with 20 mM reduced glutathione for 15 min at room temperature. Sch9 kinase assays were performed as described previously (Huber *et al*, 2009).

mRNA sequencing

RNA extracts were purified of genomic DNA contaminations using RNeasy kits (Qiagen). Libraries were prepared from pools of equivalent amounts of RNA from four independent experiments and sequenced using version 4 kits and single read flow cells on Genome Analyzer IIx machine according to the manufacturer's instructions (Illumina). Sequencing reads were mapped to the transcriptome of *S. cerevisiae* using the QSeq software with standard parameters (DNAStar). Minimal thresholds of 20 reads in each condition and 100 reads in at least one condition were applied to all transcripts. The relative expression of 5083 transcripts meeting these criteria was calculated by normalizing their reads counts to the total number of reads in each condition. A summary of the libraries' sequencing and reads mapping to yeast ORFs is shown in Supplementary Table S6. We defined as *Ribi* genes the first 500 non-*RP* genes in the ranking list of Wade *et al* (2006). Raw sequence files are available in the GEO database (http://www.ncbi.nlm.nih.gov/geo/; accession number: GSE29122).

Miller spreads

'Miller' chromatin spreads were prepared according to French *et al* (2003). All areas of the grids containing dispersed nucleoli were photographed. The number of RNA polymerase I molecules on each visible 35S rRNA gene was counted by hand on enlarged micrographs. To be included, the chromatin strand on which the gene occurred needed to be sufficiently long to encompass the entire length of the gene.

^{3}H-uracil pulse-labelling assays

^{3}H-uracil pulse-labelling assays were performed as described previously (Huber *et al*, 2009) with the following modifications. Briefly, cells were made prototroph and grown in SC-URA at 25°C. In all, 10 ml aliquots were removed and pulsed with 25 μCi ^{3}H-uracil for 20 min. Cold uracil was added at a 100-fold molar excess and cells were grown 20 more minutes before harvest and total RNA extraction. RNA was resolved by gel electrophoresis and transferred to membranes. Its loading was controlled by ethidium bromide staining and the incorporation of ^{3}H-uracil was determined by exposure to phosphorimager screens.

Quantitative western blotting

The Li-Cor infrared fluorescent system was used for quantitative western blotting. All antibodies were incubated in PBS 0.01%

Tween-20 (PBST) supplemented with 5% BSA. Washing steps were performed using PBST. After 1 h blocking in PBST 5% BSA, membranes were probed overnight with mouse anti-HA and rabbit anti-Hog1 antibodies. Membranes were washed three times with PBST and the primary antibodies were detected with anti-mouse and anti-rabbit secondary antibodies coupled to the infrared dyes IRDye800® (Rockland, PA, USA) and IRDye680® (Li-Cor, NE, USA), respectively. After three washes, fluorescence was detected using the Odyssey® IR imaging system (Li-Cor). The ImageJ software was used for quantification (Abramoff *et al*, 2004).

ChIP assays

ChIP assays were performed and quantified by qPCR using the SYBR Green system as described previously (Bianchi *et al*, 2004) with slight modifications. Briefly, cells were fixed with 1% formaldehyde for 10 min at room temperature. Fixation was stopped with 125 mM glycine and cells were harvested by centrifugation. The extracted chromatin was sheared in a bioruptor sonicator (Diagenode) for 20 min (30 s on; 30 s off) at full power. IPs were performed using pan-mouse IgG beads (Dynal, Invitrogen) and were quantified using primers (Supplementary Table S7) for the indicated loci and normalized by qPCR DNA purified from the IP input. IP efficiency was normalized with a similar quantification for the *ADH4* locus as a control.

For ChIP-Seq experiments, ChIPs were scaled up by a factor of six (240 ml of culture at an OD_{600} of 0.5) and chromatin was sheared in aliquots of 300 μl for 30 min instead of 20 with otherwise identical settings. ChIPs were repeated three times (untagged controls were repeated nine times). The immunopurified DNA was pooled, crosslinks were reversed overnight at 65°C and the DNA was purified using Qiagen PCR purification kits. The DNA was eluted with 40 μl of the supplied elution buffer and stored at −80°C until further analysis. Libraries were prepared using ChIP-Seq sample preparation kits (Illumina) according to the manufacturer's instructions. DNA fragments ends were repaired using a mix of Klenow DNA polymerase, T4 DNA polymerase and T4 polynucleotide kinase. DNA was then purified and 3′ A overhangs were added using a Klenow fragment (3′–5′ exo minus). DNA was purified again and ligated to adapters. In all, 190 ± 10 bp fragments were selected using the E-Gel SizeSelect system (Invitrogen) and purified. Fragments with adapters were finally enriched with 18 cycles of PCR and purified. High-throughput sequencing of libraries was performed on a Genome Analyzer IIx machine (Illumina) each in a separate channel. Sequencing reads were mapped on SGD1.01 genome assembly using Bowtie 0.12.1 (Langmead *et al*, 2009), with parameters *-n 3 –best –strata –solexa1.3-quals -a -m 20* and viewed with the USCS Genome Browser (Kent *et al*, 2002). Libraries sequencing and reads alignment to the yeast genome are summarized in Supplementary Table S8. The MACS algorithm v 1.7.3.1 (Zhang *et al*, 2008) was used to detect Sds3–TAP binding peaks by comparing the mapped read counts obtained from the *sch9^{as}SDS3–TAP* versus the untagged *sch9^{as}* strains with parameters *–mfold = 2 –P value = 1e−5*. Raw sequence files are available in the GEO database (GSE29124).

Supplementary data

Supplementary data are available at *The EMBO Journal* Online (http://www.embojournal.org).

Acknowledgements

We thank David Shore and RL laboratory members for comments on draft manuscripts. We are grateful for all the high-throughput sequencing performed at the Genomics platform of the National Center of Competence in Research 'Frontiers in Genetics' and their computational analysis performed at the Vital-IT Center for high-performance computing of the Swiss Institute of Bioinformatics (http://www.vital-it.ch). AH was recipient of a fellowship from the Novartis Foundation for Biology and Medicine. RL is the recipient of a professorship from the Swiss National Science Foundation (PP00P3-110770/3100A0-108114) and receives generous support from the canton of Genève, the National Centers of Competence in Research 'Frontiers in Genetics' and 'Chemical Biology', the Leenaards Foundation, and the European Research Council (ERC-2007-StG 206173-TOR signalling). ALB acknowledges funding by the NIH (GM63952). MT acknowledges support from the Wellcome Trust, a Royal Society Wolfson Research Merit Award and the Scottish Universities Life Sciences Alliance. JR is supported by the SystemsX.ch initiative and the EPFL.

Author contributions: Miller chromatin spreads were performed by SF. Cell sizes were measured by HT. SY performed western blot analyses (Supplementary Figures S5A and S6C). MS carried out western blot analysis (Figure 1B) and protein determinations by flow cytometry. MPP performed RT–qPCR measurements (Supplementary Figure S5B). High-throughput sequencing data mapping and analysis was carried out by JR. All other experiments and analyses were carried out by AH. MT, ALB and RL contributed to experimental design and supervision. AH wrote the manuscript with the help of HT, SF, MT, ALB and RL.

Conflict of interest

The authors declare that they have no conflict of interest.

References

Abramoff MD, Magalhaes PJ, Ram SJ (2004) Image processing with ImageJ. *Biophoton Int* **11:** 36–41

Badis G, Chan ET, van Bakel H, Pena-Castillo L, Tillo D, Tsui K, Carlson CD, Gossett AJ, Hasinoff MJ, Warren CL, Gebbia M, Talukder S, Yang A, Mnaimneh S, Terterov D, Coburn D, Li Yeo A, Yeo ZX, Clarke ND, Lieb JD *et al* (2008) A library of yeast transcription factor motifs reveals a widespread function for Rsc3 in targeting nucleosome exclusion at promoters. *Mol Cell* **32:** 878–887

Bianchi A, Negrini S, Shore D (2004) Delivery of yeast telomerase to a DNA break depends on the recruitment functions of Cdc13 and Est1. *Mol Cell* **16:** 139–146

Bodenmiller B, Campbell D, Gerrits B, Lam H, Jovanovic M, Picotti P, Schlapbach R, Aebersold R (2008) PhosphoPep—a database of protein phosphorylation sites in model organisms. *Nat Biotechnol* **26:** 1339–1340

Breitkreutz A, Choi H, Sharom JR, Boucher L, Neduva V, Larsen B, Lin ZY, Breitkreutz BJ, Stark C, Liu G, Ahn J, Dewar-Darch D, Reguly T, Tang X, Almeida R, Qin ZS, Pawson T, Gingras AC, Nesvizhskii AI, Tyers M (2010) A global protein kinase and phosphatase interaction network in yeast. *Science* **328:** 1043–1046

Budovskaya YV, Stephan JS, Deminoff SJ, Herman PK (2005) An evolutionary proteomics approach identifies substrates of the cAMP-dependent protein kinase. *Proc Natl Acad Sci USA* **102:** 13933–13938

Carrozza MJ, Florens L, Swanson SK, Shia W-J, Anderson S, Yates J, Washburn MP, Workman JL (2005a) Stable incorporation of sequence specific repressors Ash1 and Ume6 into the Rpd3L complex. *Biochim Biophys Acta* **1731:** 77–87

Carrozza MJ, Li B, Florens L, Suganuma T, Swanson SK, Lee KK, Shia WJ, Anderson S, Yates J, Washburn MP, Workman JL (2005b) Histone H3 methylation by Set2 directs deacetylation of coding regions by Rpd3S to suppress spurious intragenic transcription. *Cell* **123:** 581–592

Chi A, Huttenhower C, Geer LY, Coon JJ, Syka JE, Bai DL, Shabanowitz J, Burke DJ, Troyanskaya OG, Hunt DF (2007) Analysis of phosphorylation sites on proteins from Saccharomyces cerevisiae by electron transfer dissociation (ETD) mass spectrometry. *Proc Natl Acad Sci USA* **104:** 2193–2198

Deminoff SJ, Howard SC, Hester A, Warner S, Herman PK (2006) Using substrate-binding variants of the cAMP-dependent protein kinase to identify novel targets and a kinase domain important for substrate interactions in Saccharomyces cerevisiae. *Genetics* **173:** 1909–1917

De Virgilio C, Loewith R (2006) Cell growth control: little eukaryotes make big contributions. *Oncogene* **25:** 6392–6415

Ferreira-Cerca S, Poll G, Gleizes PE, Tschochner H, Milkereit P (2005) Roles of eukaryotic ribosomal proteins in maturation and transport of pre-18S rRNA and ribosome function. *Mol Cell* **20:** 263–275

Freckleton G, Lippman SI, Broach JR, Tavazoie S (2009) Microarray profiling of phage-display selections for rapid mapping of transcription factor-DNA interactions. *PLoS Genet* **5:** e1000449

French SL, Osheim YN, Cioci F, Nomura M, Beyer AL (2003) In exponentially growing Saccharomyces cerevisiae cells, rRNA synthesis is determined by the summed RNA polymerase I loading rate rather than by the number of active genes. *Mol Cell Biol* **23:** 1558–1568

Harbison CT, Gordon DB, Lee TI, Rinaldi NJ, Macisaac KD, Danford TW, Hannett NM, Tagne J-B, Reynolds DB, Yoo J, Jennings EG, Zeitlinger J, Pokholok DK, Kellis M, Rolfe PA, Takusagawa KT, Lander ES, Gifford DK, Fraenkel E, Young RA (2004) Transcriptional regulatory code of a eukaryotic genome. *Nature* **431:** 99–104

Heitman J, Movva NR, Hall MN (1991) Targets for cell cycle arrest by the immunosuppressant rapamycin in yeast. *Science* **253:** 905–909

Huber A, Bodenmiller B, Uotila A, Stahl M, Wanka S, Gerrits B, Aebersold R, Loewith R (2009) Characterization of the rapamycin-sensitive phosphoproteome reveals that Sch9 is a central coordinator of protein synthesis. *Genes Dev* **23:** 1929–1943

Hughes JD, Estep PW, Tavazoie S, Church GM (2000) Computational identification of cis-regulatory elements associated with groups of functionally related genes in Saccharomyces cerevisiae. *J Mol Biol* **296:** 1205–1214

Humphrey EL, Shamji AF, Bernstein BE, Schreiber SL (2004) Rpd3p relocation mediates a transcriptional response to rapamycin in yeast. *Chem Biol* **11:** 295–299

Jorgensen P, Nishikawa JL, Breitkreutz BJ, Tyers M (2002) Systematic identification of pathways that couple cell growth and division in yeast. *Science* **297:** 395–400

Jorgensen P, Rupes I, Sharom JR, Schneper L, Broach JR, Tyers M (2004) A dynamic transcriptional network communicates growth potential to ribosome synthesis and critical cell size. *Genes Dev* **18:** 2491–2505

Jorgensen P, Tyers M (2004) How cells coordinate growth and division. *Curr Biol* **14:** R1014–R1027

Ju Q, Warner JR (1994) Ribosome synthesis during the growth cycle of Saccharomyces cerevisiae. *Yeast* **10:** 151–157

Kasten MM, Stillman DJ (1997) Identification of the Saccharomyces cerevisiae genes STB1-STB5 encoding Sin3p binding proteins. *Mol Gen Genet* **256:** 376–386

Kent WJ, Sugnet CW, Furey TS, Roskin KM, Pringle TH, Zahler AM, Haussler D (2002) The human genome browser at UCSC. *Genome Res* **12:** 996–1006

Laferte A, Favry E, Sentenac A, Riva M, Carles C, Chedin S (2006) The transcriptional activity of RNA polymerase I is a key determinant for the level of all ribosome components. *Genes Dev* **20:** 2030–2040

Langmead B, Trapnell C, Pop M, Salzberg SL (2009) Ultrafast and memory-efficient alignment of short DNA sequences to the human genome. *Genome Biol* **10:** R25

Lee J, Moir RD, Willis IM (2009) Regulation of RNA polymerase III transcription involves SCH9-dependent and SCH9-independent branches of the target of rapamycin (TOR) pathway. *J Biol Chem* **284:** 12604–12608

Lempiainen H, Shore D (2009) Growth control and ribosome biogenesis. *Curr Opin Cell Biol* **21:** 855–863

Lempiainen H, Uotila A, Urban J, Dohnal I, Ammerer G, Loewith R, Shore D (2009) Sfp1 interaction with TORC1 and Mrs6 reveals feedback regulation on TOR signaling. *Mol Cell* **33:** 704–716

Liko D, Conway MK, Grunwald DS, Heideman W (2010) Stb3 plays a role in the glucose-induced transition from quiescence to growth in Saccharomyces cerevisiae. *Genetics* **185:** 797–810

Liko D, Slattery MG, Heideman W (2007) Stb3 binds to ribosomal RNA processing element motifs that control transcriptional responses to growth in Saccharomyces cerevisiae. *J Biol Chem* **282:** 26623–26628

Lippman SI, Broach JR (2009) Protein kinase A and TORC1 activate genes for ribosomal biogenesis by inactivating repressors encoded by Dot6 and its homolog Tod6. *Proc Natl Acad Sci USA* **106:** 19928–19933

Martin DE, Soulard A, Hall MN (2004) TOR regulates ribosomal protein gene expression via PKA and the Forkhead transcription factor FHL1. *Cell* **119:** 969–979

Mnaimneh S, Davierwala AP, Haynes J, Moffat J, Peng WT, Zhang W, Yang X, Pootoolal J, Chua G, Lopez A, Trochesset M, Morse D, Krogan NJ, Hiley SL, Li Z, Morris Q, Grigull J, Mitsakakis N, Roberts CJ, Greenblatt JF *et al* (2004) Exploration of essential gene functions via titratable promoter alleles. *Cell* **118:** 31–44

Oficjalska-Pham D, Harismendy O, Smagowicz WJ, Gonzalez de Peredo A, Boguta M, Sentenac A, Lefebvre O (2006) General repression of RNA polymerase III transcription is triggered by protein phosphatase type 2A-mediated dephosphorylation of Maf1. *Mol Cell* **22:** 623–632

Peyroche G, Milkereit P, Bischler N, Tschochner H, Schultz P, Sentenac A, Carles C, Riva M (2000) The recruitment of RNA polymerase I on rDNA is mediated by the interaction of the A43 subunit with Rrn3. *EMBO J* **19:** 5473–5482

Philippi A, Steinbauer R, Reiter A, Fath S, Leger-Silvestre I, Milkereit P, Griesenbeck J, Tschochner H (2010) TOR-dependent reduction in the expression level of Rrn3p lowers the activity of the yeast RNA Pol I machinery, but does not account for the strong inhibition of rRNA production. *Nucleic Acids Res* **38:** 5315–5326

Poll G, Braun T, Jakovljevic J, Neueder A, Jakob S, Woolford Jr JL, Tschochner H, Milkereit P (2009) rRNA maturation in yeast cells depleted of large ribosomal subunit proteins. *PLoS One* **4:** e8249

Ramachandran V, Herman PK (2011) Antagonistic interactions between the cAMP-dependent protein kinase and Tor signaling pathways modulate cell growth in Saccharomyces cerevisiae. *Genetics* **187:** 441–454

Reiter A, Steinbauer R, Philippi A, Gerber J, Tschochner H, Milkereit P, Griesenbeck J (2011) Reduction in ribosomal protein synthesis is sufficient to explain major effects on ribosome production after short-term TOR inactivation in Saccharomyces cerevisiae. *Mol Cell Biol* **31:** 803–817

Roberts DN, Wilson B, Huff JT, Stewart AJ, Cairns BR (2006) Dephosphorylation and genome-wide association of Maf1 with Pol III-transcribed genes during repression. *Mol Cell* **22:** 633–644

Rohde JR, Cardenas ME (2003) The tor pathway regulates gene expression by linking nutrient sensing to histone acetylation. *Mol Cell Biol* **23:** 629–635

Rudra D, Zhao Y, Warner JR (2005) Central role of Ifh1p-Fhl1p interaction in the synthesis of yeast ribosomal proteins. *EMBO J* **24:** 533–542

Schawalder SB, Kabani M, Howald I, Choudhury U, Werner M, Shore D (2004) Growth-regulated recruitment of the essential yeast ribosomal protein gene activator Ifh1. *Nature* **432:** 1058–1061

Shevchenko A, Roguev A, Schaft D, Buchanan L, Habermann B, Sakalar C, Thomas H, Krogan NJ, Stewart AF (2008) Chromatin central: towards the comparative proteome by accurate mapping of the yeast proteomic environment. *Genome Biol* **9:** R167

Shokat K, Velleca M (2002) Novel chemical genetic approaches to the discovery of signal transduction inhibitors. *Drug Discov Today* **7:** 872–879

Singh J, Tyers M (2009) A Rab escort protein integrates the secretion system with TOR signaling and ribosome biogenesis. *Genes Dev* **23:** 1944–1958

Soulard A, Cremonesi A, Moes S, Schutz F, Jeno P, Hall MN (2010) The rapamycin-sensitive phosphoproteome reveals that TOR controls protein kinase A toward some but not all substrates. *Mol Biol Cell* **21:** 3475–3486

Stark C, Su T-C, Breitkreutz A, Lourenco P, Dahabieh M, Breitkreutz B-J, Tyers M, Sadowski I (2010) PhosphoGRID: a database of experimentally verified *in vivo* protein phosphorylation sites from the budding yeast Saccharomyces cerevisiae. *Database* **2010:** bap026

Upadhya R, Lee J, Willis IM (2002) Maf1 is an essential mediator of diverse signals that repress RNA polymerase III transcription. *Mol Cell* **10:** 1489–1494

Urban J, Soulard A, Huber A, Lippman S, Mukhopadhyay D, Deloche O, Wanke V, Anrather D, Ammerer G, Riezman H, Broach JR, De Virgilio C, Hall MN, Loewith R (2007) Sch9 is a major target of TORC1 in Saccharomyces cerevisiae. *Mol Cell* **26:** 663–674

Wade CH, Umbarger MA, McAlear MA (2006) The budding yeast rRNA and ribosome biosynthesis (RRB) regulon contains over 200 genes. *Yeast* **23:** 293–306

Wade JT, Hall DB, Struhl K (2004) The transcription factor Ifh1 is a key regulator of yeast ribosomal protein genes. *Nature* **432:** 1054–1058

Warner JR (1999) The economics of ribosome biosynthesis in yeast. *Trends Biochem Sci* **24:** 437–440

Wei Y, Zheng XF (2009) Sch9 partially mediates TORC1 signaling to control ribosomal RNA synthesis. *Cell Cycle* **8:** 4085–4090

Yorimitsu T, Zaman S, Broach JR, Klionsky DJ (2007) Protein kinase A and Sch9 cooperatively regulate induction of autophagy in Saccharomyces cerevisiae. *Mol Biol Cell* **18:** 4180–4189

Zaman S, Lippman SI, Zhao X, Broach JR (2008) How Saccharomyces responds to nutrients. *Ann Rev Genet* **42:** 27–81

Zaragoza D, Ghavidel A, Heitman J, Schultz MC (1998) Rapamycin induces the G0 program of transcriptional repression in yeast by interfering with the TOR signaling pathway. *Mol Cell Biol* **18:** 4463–4470

Zhang Y, Liu T, Meyer C, Eeckhoute J, Johnson D, Bernstein B, Nusbaum C, Myers R, Brown M, Li W, Liu XS (2008) Model-based analysis of ChIP-Seq (MACS). *Genome Biol* **9:** R137

Zhu C, Byers K, McCord R, Shi Z, Berger M, Newburger D, Saulrieta K, Smith Z, Shah M, Radhakrishnan M, Philippakis A, Hu Y, De Masi F, Pacek M, Rolfs A, Murthy T, Labaer J, Bulyk ML (2009) High-resolution DNA binding specificity analysis of yeast transcription factors. *Genome Res* **19:** 556–566

